Chapter 12

Genetic Algorithm and Simulated Annealing: A Combined Intelligent Optimization Method and Its Application to Subsynchronous Damping Control in Electrical Power Transmission Systems

Xiaorong Xie

Additional information is available at the end of the chapter

http://dx.doi.org/10.5772/50371

1. Introduction

Series compensations (SCs) have been widely used in electrical power systems to enhance transmission capability through partial compensation of line reactors. However, they will trigger oscillatory modes inherent in the mass-spring system of turbine-generators, resulting in subsynchronous resonance (SSR), which, if not properly handled, could cause shaft failure. The SSR phenomenon was first discussed in 1937 [1] and until 1971, shaft torsional oscillations were ignored. Two shaft failures at the Mohave power plant in Southern Nevada, USA [2] led to the understanding and development of the theory of interaction between series-capacitor compensated lines and the torsional modes of steam turbine-generators. After the second shaft failure at Mohave, the utility industry devoted considerable effort to the analysis and suppression of SSR. Much has been written on the subject as evidenced by the bibliography [3] and three supplements [4, 5, 6]. Generally, when preliminary analysis shows the system to be at risk of unstable SSR, control measures must be applied [7]. In this chapter, two types of controllers, namely, supplementary excitation damping control (SEDC) and static var compensator based subsynchronous damping control (SVC-SSDC), are used for the mitigation of SSR problem. The emphasis of our work is to achieve an optimal design of the controller parameters with the proposed genetic algorithm and simulated annealing (GA-SA) algorithm.

The SSR issue is generally addressed under three different types [8]: induction generator effect (IGE), torsional interaction (TI), and torque amplification (TA). In all cases, SSR is due to the interaction of a series capacitor compensated system with a turbine-generator.

However, this chapter will focus on the TI type SSR, because it is the main problem we encountered in practice.

TI-SSR is the interplay between the mechanical shaft system (turbine-generator) and the series- capacitor compensated electrical network. Small-signal disturbances in a power system result in simultaneous excitation of all natural modes of the electrical and mechanical systems. The turbine-generator shaft system responds to disturbances with oscillations at its torsional natural frequencies. Therefore, TI-SSR can be viewed as a stability phenomenon of the linearized system model [9-10]. In other words, their stability and design of control parameter can be investigated with the eigenvalues of the small-signal model obtained at a certain working point [10]. In our study, for each of the concerned operation conditions, a detailed linearized system model of the studied system is developed. It can be expressed as

$$\begin{cases} \Delta\dot{\mathbf{X}} = \mathbf{A}\Delta\mathbf{X} + \mathbf{B}\Delta\mathbf{U} \\ \Delta\mathbf{Y} = \mathbf{C}\Delta\mathbf{X} \end{cases} \tag{1}$$

Where $\Delta\mathbf{X}$ is the state vector, $\Delta\mathbf{U}$ is the input vector and $\Delta\mathbf{Y}$ is the output or feedback vector.

In model (1), the following various sub-models are included:

- the lumped mass-spring model of the mechanical shaft system of the turbine-generator set;
- the electromagnetic model of the generator, which is generally represented with the dq0 model with three damper windings [11, 12];
- the excitation system, for instance, the static self-parallel excitation system is modeled with the IEEE ST4B-type automatic voltage regulator (AVR) and PSS2B-type power system stabilizer (PSS);
- the model of the electrical network, incorporating the lines, transformers and the series capacitors.

The controller, either the SEDC or the SVC-SSDC to be discussed, can be also be linearized as

$$\begin{cases} \Delta\dot{\mathbf{Z}} = \mathbf{F}(\boldsymbol{\alpha})\Delta\mathbf{Z} + \mathbf{G}(\boldsymbol{\alpha})\ \Delta\mathbf{Y} \\ \Delta\mathbf{U} = \mathbf{H}(\boldsymbol{\alpha})\Delta\mathbf{Z} \end{cases} \tag{2}$$

where $\Delta\mathbf{Z}$ is the state vector, and $\mathbf{F},\mathbf{G},\mathbf{H}$ are the coefficient matrices with appropriate dimensions and their elements are determined by the control parameter vector $\boldsymbol{\alpha}$, which including the gains and time constants of the controller to be designed.

Therefore the close-loop system model under a certain operation situation can be obtained by combining the open-loop system model (1) and the controller (2), i.e.

$$\Delta\dot{\hat{\mathbf{X}}} = \hat{\mathbf{A}}\Delta\hat{\mathbf{X}} \tag{3}$$

where $\Delta\hat{\mathbf{X}} = \begin{bmatrix} \Delta\mathbf{X} & \Delta\mathbf{Z} \end{bmatrix}^{\mathrm{T}}$ is the extended state vector and $\hat{\mathbf{A}} = \begin{bmatrix} \mathbf{A} & \mathbf{BH} \\ \mathbf{GC} & \mathbf{F} \end{bmatrix}$ is the extended coefficient matrix with appropriate dimensions.

Obviously, the eigenvalues of the matrices $\mathbf{A}$ and $\hat{\mathbf{A}}$ that correspond to the torsional modes represent the stability or damping of these TI modes for the open-loop and closed-loop systems respectively. Hence, by the eigen-analysis method, the relationship between the torsional damping with system variables and control parameters can be traced out under different operating conditions. Generally, for an uncontrolled practical series-compensated power system, several of the eigenvalues related to the TI-SSR problem would be negative or unstable under certain operating conditions, i.e., the SSR problem is a multimodal one. Thus, the key issue is to design an effective control strategy which can meet the following requirements: First, the multimodal SSR must be damped simultaneously and the controller parameters determined in a coordinated way. Second, the controller must be robust enough to stabilize SSR under all possible operating conditions. In addition, the controller should be practical, i.e., easy to implement and operate. Finally, its size and operational loss should be reasonable for reduction of cost, room and maintenance.

In this chapter, the aimed power system and its SSR problem is represented with detailed electromagnetic models and the task of control-design is formulated into the constrained nonlinear optimization problem, which is of the following form:

$$\begin{aligned} &\max f \\ &\text{subject to: } \underline{\boldsymbol{\Gamma}}(\boldsymbol{\alpha}) \le \boldsymbol{\Gamma}(\boldsymbol{\alpha}) \le \overline{\boldsymbol{\Gamma}}(\boldsymbol{\alpha}) \end{aligned} \tag{4}$$

Where f is the fitness function to be optimized, $\boldsymbol{\Gamma}(\boldsymbol{\alpha})$ is the function of the control parameter $\boldsymbol{\alpha}$, which has its lower and upper limits being $\underline{\boldsymbol{\Gamma}}(\boldsymbol{\alpha})$, $\overline{\boldsymbol{\Gamma}}(\boldsymbol{\alpha})$ respectively.

For our concerned multimodal SSR problem, the fitness function is generally defined as [13]

$$\begin{aligned} f &= \sum_{i=1}^{N} w_i \eta_i + w_{N+1} \min\{\eta_1, \eta_2, \eta_3\}, \sum_{i=1}^{N+1} w_i = 1, w_i > 0 \\ \eta_i &= \min_{j=1}^{j=M} \left\{ \sigma_{ij} \right\},\ \sigma_{ij} = -\mathrm{Re}(\lambda_{ij}) / \left| \mathrm{Im}(\lambda_{ij}) \right|, \\ \lambda_{ij} &= \lambda_i \left\{ \hat{A}_j(\boldsymbol{\alpha}) \right\}; i = 1,2,3; j = 1,...,M \end{aligned} \tag{5}$$

where $\hat{\mathbf{A}}_j$ is the closed-loop coefficient matrix for the *j*-th operating condition and is jointly determined by the system variables and the control parameters; $\lambda_i\{\cdot\}$ means the calculation of the *i*-th SSR mode of the included close-loop coefficient matrix; $\mathrm{Re}(\lambda_{ij})$ and $\mathrm{Im}(\lambda_{ij})$ are the real and imaginary parts of the SSR mode; σ_{ij} is the close-loop damping; η_i is the least damping among all operating conditions; w_i are the positive weight coefficients; N is the number of concerned SSR modes; M is the number of small-signal system model with each representing an evaluation condition; the subscripts *i*, *j* denote the index of the SSR mode and the operating condition respectively.

The control-design problem can be summarized as follows:

Firstly, for a SSR-threatened system, representative conditions should be selected as the "evaluation conditions", which cover the full range of generator output levels as well as the status of transmission lines. While these evaluation conditions by no means limit the situations under which the power system operates, together they form the edge of practical operating conditions and the most unfavorable situations relevant to the controller to be designed. Therefore, the derived controller can be robust enough to stabilize the system under all possible conditions.

Secondly, for each evaluation condition, a linearized model like (1)-(3) is derived for the nonlinear system as well as the controller via small-signal approximation, and the damping of torsional modes can be calculated by eigen-analysis. Consequently, the parameter sensitivity of the control on the stability of TI-type SSR is quantified.

Thirdly, the control-design task, i.e., simultaneously tuning of the control parameters, was formulated into a standard nonlinear optimization problem as described in (4)-(5), by appropriately determining the fitness function and the constraints on the parameters of the controller. As seen in (5), the ability of the controller to depress SSR is determined by the weighted sum of the damping of concerned torsional modes under all listed conditions. Furthermore, the least damped one is emphasized with additional weight to achieve better damping.

Next, by solving the optimization problem (4)-(5), the control parameters can be tuned simultaneously and an optimal control strategy to mitigate the SSR issue is obtained.

Finally, the designed controller should be verified with simulation study on the nonlinear system model, or even be implemented as hardware equipment and tested in practical applications.

2. The combined intelligent optimization method: Genetic algorithm and simulated annealing (GA-SA)

The control-design problem (4)-(5) is a complex nonlinear optimization problem with many models, each corresponding to an evaluation condition. However, it is difficult for conventional methods due to its nonlinear nature and high dimension of the solution space. Here, we provide the solution by combining genetic algorithm (GA) and simulated annealing (SA), termed GA-SA. As a hybrid and global optimization strategy, GA-SA takes advantage of both GA's parallel-searching capability and SA's probabilistic jumping property [14-17]: The fast and global parallel searching ability of GA is retained, and the diversity is improved by SA state transition. Thus, premature convergence in GA can be avoided. Furthermore, SA renders GA mutation more controllable by its temperature. Thanks to the powerful global searching ability, the criteria for the selection of algorithm parameters are very much relaxed, resulting in improved performance and robust optimization. Since the basic principle of GA-SA has been well documented [14-17], only the

particular procedures employed to design the SSR control (i.e., SEDC and SVC-SSDC) are elaborated in the following.

The flow chart of the proposed GA-SA is shown in Fig. 1.

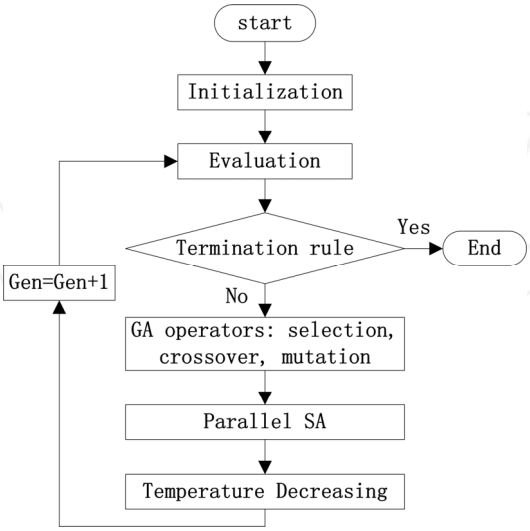

Figure 1. Flow chart of the implemented GA-SA

The GA-SA is executed with the following steps.

Step 1. GA-SA initialization.

i. Define algorithm parameters, including: boundaries of control parameters, GA parameters (population size n, number of generations k_{GA}, number of preferential chromosomes n_b, crossover probability p_c, mutation probability p_m, initial perturbation amplitude ξ_{GA0})and SA parameters (number of state transition k_{SA}, cooling rate r, perturbation amplitude ξ_{SA0}, initial acceptance rate p_r).

ii. Set an initial population by randomly generating n feasible vectors or chromosomes in a reasonable range of the control parameters;

iii. Define the initial temperature as $t_0 = -\Delta_{\max} / \ln p_r$, where $\Delta_{\max} = |f_{\max} - f_{\min}|$ and $f_{\max}, f_{\min}$ are fitness values of the best and the worst chromosomes of the initial population.

Step 2. Evaluate each chromosome by using the fitness function.

Step 3. Apply GA operations to generate a new generation. This is fulfilled with three sub-operators:

i. Selection: Select n_b chromosomes as potential parents from the old population. The selection is simulated by spinning a weighted roulette wheel [18] in such a way that the fittest chromosomes have a higher probability of being selected, so that their genes have a greater chance to be passed on to the next generation.

ii. Crossover: This is carried out between each parent member (p_i, i=1,…,n_b) and the fittest chromosome (p_0) of the current generation. The convex crossover method is adopted to produce the offspring x_{i1}, x_{i2}, where $x_{i1} = \lambda p_i + (1-\lambda)p_0$, $x_{i2} = (1-\lambda)p_i + \lambda p_0$, $0 < \lambda < 1$ [17]. All offspring are added to the original population and then n chromosomes of higher fitness are chosen to form a new generation.

iii. Mutation with one elite reservation strategy: Keep the best chromosome and apply mutation to other chromosomes with a probability of p_m. For each mutation, a new chromosome x_n is generated from an old chromosome x_o by applying a random perturbation, i.e., $x_n = x_o + m\xi_{GA}$, where $m \in (-5,5)$ is a random variable of Cauchy distribution, and ξ_{GA} is the perturbation amplitude.

Step 4. Apply the parallel SA algorithm to enhance the quality of the new population. State transition and acceptance are repeatedly used during the SA.

i. State transition: First, SA selects candidate chromosomes from the GA-generated population according to the roulette strategy [18]. State transition is then performed k_{SA} times for each of these chromosomes. The operation of state transition is identical to that of GA mutation, the only difference being that the former has a much smaller parameter of perturbation amplitude ξ_{SA}.

ii. State acceptance: Let f_i and f_{i+1} be the fitness values of the original state x_i and the state x_{i+1} obtained by state transition, respectively. If $f_{i+1} > f_i$, x_{i+1} is accepted as the starting point for the next state transition; otherwise, x_{i+1} is accepted with probability $p = \exp[(f_i - f_{i+1})/T_p]$.

Step 5. Cooling: As the optimization proceeds, the temperature T_p is dynamically updated according to the rule $Tp_{k+1} = r\ Tp_k$. Thus, at higher temperatures, SA will accept poorer status with certain probability to avoid plugging into local minimum; while at lower temperatures, it basically turns out to be an optimization function in small random searches.

Step 6. Termination: GA-SA terminates if the maximum number of generations allowed (k_{GA}) is reached or the best result has not seen improvement for a certain number of generations. Otherwise, go back to Step 2.

3. Application of GA-SA for SEDC optimization

3.1. The target system

The Shangdu power plant (SPP), located in the Inner Mongolia Autonomous Region, is about 300 kilometers north of Beijing city. It has four 600 MW steam turbine-generators connected to the North China Power Grid through 500 kV transmission lines, including the 243 km double lines connecting SPP with the Chengde substation and the 130km double lines connecting the Chengde substation with the Jiangjiaying substation. Fig.2 illustrates the one-line diagram of the equivalent transmission system. To improve the transferring capability as well as system stability, fixed series capacitors (FSCs) are applied to the parallel transmission lines between SPP and the Chengde substation with 45% compensation degree. The four turbine-generators are subcritical air-cooled machines with

almost the same parameters. Each turbine-generator consists of four rotors, i.e., a high-and-intermediate-pressure (HIP) turbine rotor, two low-pressure (LPA and LPB) turbine rotors, and the generator rotor, thus resulting in three subsynchronous torsional modes. The characteristic frequencies (in Hz) are 15.19~15.33 (mode 1), 26.01~26.12 (mode 2) and 30.25~30.54 (mode 3). To solve the SSR problem, torsional stress relays (TSRs) and supplementary excitation damping controllers (SEDCs) are applied to the SPP generators (as shown in fig. 2).

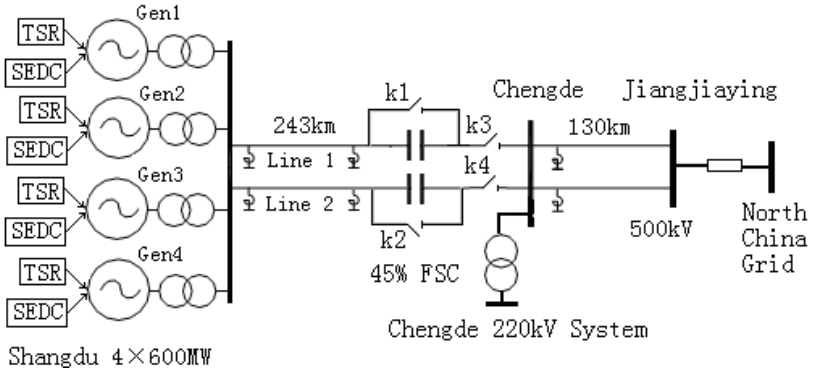

Figure 2. The one-line diagram of the equivalent transmission system

3.2. The SSR problem

A thorough evaluation of the severity of the SSR problem was conducted under all possible system conditions [19, 20], which comprised frequency scanning, eigenvalue analyses and electromagnetic transient (EMT).

With eigenvalue analysis, the modal damping (i.e., the negative real part of the torsional eigenvalue, which is a combined outcome of mechanical and electrical damping) can be obtained with respect to different operating conditions. To illustrate, 24 representative conditions are selected as the "evaluation conditions" (listed in Table 1), which cover the full range of generator output levels as well as the status of the Shangdu-Chengde lines. Table 1 also lists the calculated modal damping. Thus, the severity of SSR is quantified and the most risky situations are identified.

Through the evaluation study, characteristics of the SSR problem are summarized as follows:

i. Mode 1 is well-damped in all operating conditions; however, modes 2 and 3 may be under-damped or even unstable under some conditions. Thus, the SSR problem is a multimodal one.
ii. Mode 2 is the worst damped and tends to be unstable for numbers of operating conditions, especially when only one Shangdu-Chengde line is in service or the generator output is relatively low (corresponding to a lower mechanical damping).

iii. Modal damping is affected by several factors and each torsional mode has a most undesirable (or least damped) condition unique to its own, making it a challenge to design a controller adaptable to all operating conditions.

Oper. Cond. #	Generator output (%)				Status of SPP-Chengde lines		Mode 1 (s^{-1})	Mode 2 (s^{-1})	Mode 3 (s^{-1})
	Gen 1	Gen 2	Gen 3	Gen 4	Line 1	Line 2	No SEDC	No SEDC	No SEDC
1	0	0	0	0	online	offline	0.0312	**-0.5603**	0.0211
2	0	0	0	0	online	online	0.0367	**-0.0429**	**-0.0053**
3	0	0	0	offline	online	offline	0.0338	**-0.1992**	**-0.0764**
4	0	0	0	offline	online	online	0.0380	0.0449	0.0236
5	0	0	offline	offline	online	offline	0.0402	**-0.0235**	**-0.0921**
6	0	0	offline	offline	online	online	0.0442	0.0628	0.0290
7	0	offline	offline	offline	online	offline	0.0506	0.0594	0.0267
8	0	offline	offline	offline	online	online	0.0533	0.0796	0.0325
9	40	40	40	40	online	offline	0.0598	**-0.4887**	0.0511
10	40	40	40	40	online	online	0.0654	0.0383	0.0242
11	40	40	40	offline	online	offline	0.0590	**-0.1882**	0.0229
12	40	40	40	offline	online	online	0.0641	0.0569	0.0460
13	40	40	offline	offline	online	offline	0.0599	**-0.0123**	**-0.0864**
14	40	40	offline	offline	online	online	0.0646	0.0748	0.0567
15	40	offline	offline	offline	online	offline	0.0664	0.0684	0.0529
16	40	offline	offline	offline	online	online	0.0717	0.0916	0.0620
17	100	100	100	100	online	offline	0.0674	**-0.5455**	0.1344
18	100	100	100	100	online	online	0.0716	0.0787	0.1026
19	100	100	100	offline	online	offline	0.0615	**-0.1835**	0.1035
20	100	100	100	offline	online	online	0.0648	0.1015	0.1284
21	100	100	offline	offline	online	offline	0.0555	0.0248	**-0.0192**
22	100	100	offline	offline	online	online	0.0580	0.1226	0.1409
23	100	offline	offline	offline	online	offline	0.0511	0.1163	0.1370
24	100	offline	offline	offline	online	online	0.0540	0.1414	0.1467

Table 1. Torsional damping of the open-loop system under the evaluation conditions

3.3. Supplementary Excitation Damping Controller

SEDC is a real-time control system that works through the excitation system by modulating the field voltage at the torsional frequencies. Fig.3 illustrates the signal relationship of the SEDC, the excitation regulators, the generators and the grid. As a supplementary control loop, SEDC uses the mechanical speed of the HIP turbine (ω_1) as the only feedback signal to generate the subsynchronous control output (u_{SEDC}). u_{SEDC} is then added to the output of AVR (u_C) to form a modulated control signal (u_f), which

drives the excitation circuit to yield the field voltage (E_f). There is a time delay (τ) between u_f and E_f, mainly due to signal sampling, data processing and thyristor transport lag. This time delay, generally several to a dozen milliseconds, is important to the practicality of SEDC's design, since it is comparable with the period of torsional modes, which, if not taken into consideration, would deteriorate or even destabilize the SEDC-controlled system.

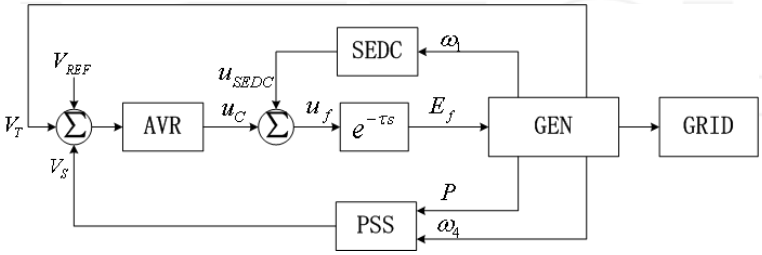

Figure 3. The signal relationship of the SEDC and the excitation regulators
(AVR: automatic voltage regulator, PSS: power system stabilizer)

Fig.4 shows the block diagram of the proposed SEDC. The mechanical speed of the HIP turbine provides the input, which after proper filtering and conditioning becomes the deviation signal $\Delta\omega_1$. It then passes through three separate control paths. Each control path, tuned to a specific mode, comprises a band-pass filter, an amplifier G_k and a unity-gain phase-shifter $(1-T_k s)^2/(1+T_k s)^2$ to generate the control signal for the corresponding mode. The control signals of all torsional modes are summarized, clipped and finally added to the AVR output to modulate the field voltage. Consequently, three subsynchronous components are generated in the excitation current, which in turn produce subsynchronous torque upon the generator shafts. If the gains and phase-shifts are appropriately set, this torque provided by SEDCs will play a role in damping SSR. So proper determination of the gains and time constants, i.e., $G_k, T_k (k=1,2,3)$ in Fig.4, is crucial to mitigate the multimodal SSR.

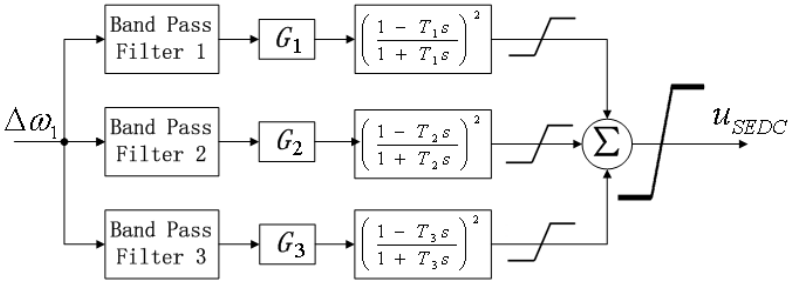

Figure 4. Configuration of SEDC

3.4. System modeling

3.4.1. The linearized open-loop system model

The linearized state equations of the four generators and network around a specific operating point can be expressed by (1). Here the state vector $\Delta\mathbf{X}$, input vector $\Delta\mathbf{U}$ and output vector $\Delta\mathbf{Y}$ are given respectively by $\Delta\mathbf{X}^{\mathrm{T}}=\left[\Delta\boldsymbol{\delta}_{4\times1}\ \ \Delta\boldsymbol{\omega}_{4\times1}\ \ \Delta\mathbf{i}_{6\times1}\ \ \Delta\mathbf{u}_{Cd,q}\right]$, $\Delta\mathbf{U}^{T}=\Delta E_f$, $\Delta\mathbf{Y}^{\mathrm{T}}=\Delta\mathbf{X}^{\mathrm{T}}$, where $\boldsymbol{\delta}_{4\times1}$ are the mass angles; $\boldsymbol{\omega}_{4\times1}$ are the mass speeds; $\mathbf{i}_{6\times1}$ are the winding currents; $\mathbf{u}_{Cd,q}$ are the *d*-axis and *q*-axis voltages of the series capacitors; E_f is the field excitation voltage and $\mathbf{A},\mathbf{B},\mathbf{C}$ are the coefficient matrices with proper dimensions.

3.4.2. The combined system model

From a combination of the models of the grid, the generators and the excitation control system, the close-loop system model can be derived (shown in Fig.3). For the convenience of further analysis and synthesis, the time delay $e^{-\tau s}$ is replaced with a rational approximation in the frequency domain, i.e. $e^{-\tau s}\cong(1+\tau s/2)^{-2}$. For the target system, the time delay τ is measured to be about 7 milliseconds. Since our SEDC scheme is actually a linear dynamic stabilizer, whose transfer function can be expressed with the general form as in (2). Therefore the close-loop system model (3) can be obtained by combining the open-loop system model and the SEDC controller.

3.5. Optimal design of SEDC based on GA-SA

For the Shangdu system, the evaluation conditions listed in Table 1 are used again for the purpose of parameters-tuning because these selected conditions together not only bound the range of practical operating conditions but also incorporate the most unfavorable situations. An SEDC based on these conditions will be robust enough to stabilize the system under all normal conditions. Then the nonlinear optimization problem can be formulated as in (4)-(5), in which the control parameter set $\boldsymbol{\alpha}=\left\{G_1,G_2,G_3,T_1,T_2,T_3\right\}$, N=3, M=24. During the parameter-tuning process, the gains and time constants of SEDC should be restricted within a reasonable range due to the control energy and hardware implementation limits. Thus the constraint can be written as

$$G_{\mathrm{lb,k}}\le G_k\le G_{\mathrm{ub},i},\ T_{\mathrm{lb,k}}\le T_k\le T_{\mathrm{ub,k}} \tag{6}$$

where $G_{\mathrm{lb,k}},G_{\mathrm{ub,k}},T_{\mathrm{lb,k}},T_{\mathrm{ub,k}}$ are the lower and upper bounds of the gains and time constants.

Then the GA-SA is adopted to solve the problem. The following algorithm parameters have been chosen after running a number of trials: The weights in the fitness function: $w_1=w_2=w_3=0.2$, $w_4=0.4$; population size = 20; crossover rate = 0.9; mutation rate = 0.1; number of generations = 30; cooling rate=0.95; and initial temperature = $-1*\Delta f/\log_{10}(0.1)$, where Δf is the maximum margin of the fitness value of the initial population.

In our case, it is discovered that the performance of GA-SA is not very sensitive to these parameters. In fact, if the population size and the number of generations are chosen properly, GA-SA will generally converge to satisfactory results after running 8 to 12 iterations, which lasts only several minutes on a modern computer. The typical convergence characteristic of the GA-SA is displayed in Fig.5. The most time-consuming step during the optimization process is the calculation of the fitness function, which is essentially the close-loop damping of the torsional modes. Therefore, a highly efficient and reliable algorithm should be used to calculate the fitness function. In this aspect, the implemented GA-SA works very well. Table 2 lists the optimized SEDC parameters obtained by the proposed GA-SA.

G_1	T_1	G_2	T_2	G_3	T_3
-378.99	0. 0535	311.45	0.0174	239.92	0.0018

Table 2. The optimized SEDC parameters

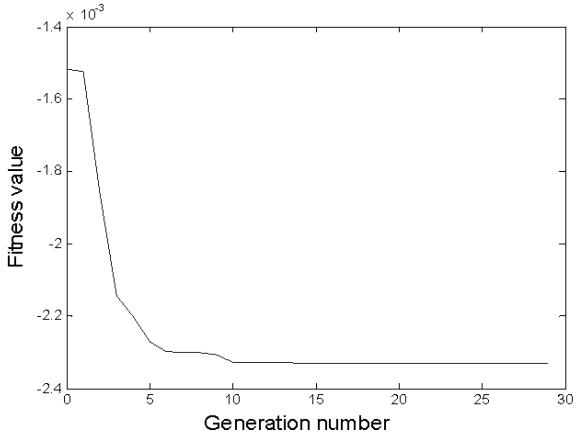

Figure 5. Convergence of the GA-SA algorithm

3.6. Performance verification of the designed SEDC

3.6.1. Model study

To verify the tuned SEDC, both eigenvalue analysis and EMT simulation were fulfilled on the close-loop system.

Eigenvalue analysis was conducted under the evaluation conditions, first in the absence and then in the presence of SEDC. The result is presented in Table 3. It shows that, without SEDC, modes 2 and 3 will incur negative damping, resulting in an unstable system. When SEDC is included into the control loop, the damping of torsional modes under all the specified conditions has been increased considerably and all unstable cases have been well stabilized.

To investigate how well the proposed controller can withstand large disturbances such as short-circuit faults, the nonlinear power system was simulated using EMT software "PSCAD/EMTDC". Step-by-step time-domain electromagnetic simulations were conducted to check the response of the SEDC controlled system during large disturbances.

In both of the two simulation experiments conducted, one Shangdu-Chengde line suffered a serious three-phase short-circuit fault. The faulting line was tripped 70 milliseconds later. In Experiment 1 all generators were 40% loaded while in Experiment 2 all generators were fully loaded. The result is summarized in Fig.6. As is shown in (a) and (c) of Fig. 6, in the absence of SEDC, the diverging delta mechanical speed of the high-pressure turbine indicates that the generators have a growing torsional vibration, which would probably lead to great damage on the shafts. When SEDC is applied in Fig.11 (b) and (d), subsynchronous oscillations in both experiments are successfully damped out.

Besides these two experiments, sufficient simulations have been carried out under other operating conditions and with large but different disturbances. Generally, SEDC is effective in improving the damping of all torsional modes and can satisfactorily mitigate the vibrations caused by SSR in large disturbances.

3.6.2. Practical applications and field tests

After extensive laboratory tests, the proposed SEDC was then applied to the practical SSR problem of the target system. By the end of October 2008, all SEDCs were put into their places. The two FSCs of the Shangdu-Chengde lines were also ready for operation. Then, to further validate the effectiveness of the proposed countermeasure, the project team conducted a series of joint tests on the SEDCs and the series-compensated system. By planned operations of SEDCs, generators, series capacitors and transmission lines, the dynamic characteristics of SSR and the response of the SEDCs were fully investigated. To save space, only some typical test results, to illustrate the function of SEDC in damping TI-SSR, are discussed hereafter.

The initial operating condition of the tested system was as follows: Units 1, 2 and 4 were online and half-loaded; Unit 3 was out of service; both Shangdu-Chengde lines were in operation; FSCs were out of service but ready for operation.

a. Switching on/off FSCs with/without SEDC

First, with all SEDCs in service, the two FSCs were switched on and then they were switched off one by one. During these operations, the torsional oscillation was observed in real time and each operation was initiated only after the dynamics that was triggered by the previous operation completely died away. The next stage involved quitting all SEDCs and repeating the above switch-on/off operations of FSCs. The mode-2 dynamics of this test is depicted in Fig.7. It can be observed that the torsional oscillation of the online machines are convergent under both the SEDC-off and the SEDC-on conditions; while the SEDC can considerably improve the modal damping and make the oscillation converge much more quickly.

Oper. Cond. #	Generator output (%)				Status of SPP-Chengde lines		Mode 1 (s^{-1})		Mode 2 (s^{-1})		Mode 3 (s^{-1})	
	Gen 1	Gen 2	Gen 3	Gen 4	Line 1	Line 2	No SEDC	With SEDC	No SEDC	With SEDC	No SEDC	With SEDC
1	0	0	0	0	online	offline	0.0312	0.0515	**-0.5603**	0.0873	0.0211	0.1078
2	0	0	0	0	online	online	0.0367	0.0571	**-0.0429**	0.1074	**-0.0053**	0.0830
3	0	0	0	offline	online	offline	0.0338	0.0783	**-0.1992**	0.1381	**-0.0764**	0.1286
4	0	0	0	offline	online	online	0.0380	0.0632	0.0449	0.1148	0.0236	0.0864
5	0	0	offline	offline	online	offline	0.0402	0.0827	**-0.0235**	0.1426	**-0.0921**	0.2030
6	0	0	offline	offline	online	online	0.0442	0.0670	0.0628	0.1395	0.0290	0.0690
7	0	offline	offline	offline	online	offline	0.0506	0.0833	0.0594	0.1145	0.0267	0.0782
8	0	offline	offline	offline	online	online	0.0533	0.0694	0.0796	0.1051	0.0325	0.0554
9	40	40	40	40	online	offline	0.0598	0.0897	**-0.4887**	0.1926	0.0511	0.1312
10	40	40	40	40	online	online	0.0654	0.0966	0.0383	0.3859	0.0242	0.1022
11	40	40	40	offline	online	offline	0.0590	0.0910	**-0.1882**	0.4687	0.0229	0.1761
12	40	40	40	offline	online	online	0.0641	0.0973	0.0569	0.3889	0.0460	0.0890
13	40	40	offline	offline	online	offline	0.0599	0.0945	**-0.0123**	0.4788	**-0.0864**	0.2073
14	40	40	offline	offline	online	online	0.0646	0.1002	0.0748	0.3812	0.0567	0.0874
15	40	offline	offline	offline	online	offline	0.0664	0.1039	0.0684	0.4095	0.0529	0.0774
16	40	offline	offline	offline	online	online	0.0717	0.0889	0.0916	0.3418	0.0620	0.0877
17	100	100	100	100	online	offline	0.0674	0.1008	**-0.5455**	0.0958	0.1344	0.2122
18	100	100	100	100	online	online	0.0716	0.1076	0.0787	0.5216	0.1026	0.2274
19	100	100	100	offline	online	offline	0.0615	0.0985	**-0.1835**	0.5564	0.1035	0.2470
20	100	100	100	offline	online	online	0.0648	0.1044	0.1015	0.5413	0.1284	0.2119
21	100	100	offline	offline	online	offline	0.0555	0.0974	0.0248	0.6364	**-0.0192**	0.3600
22	100	100	offline	offline	online	online	0.0580	0.1022	0.1226	0.5553	0.1409	0.2083
23	100	offline	offline	offline	online	offline	0.0511	0.0997	0.1163	0.6081	0.1370	0.2097
24	100	offline	offline	offline	online	online	0.0540	0.1038	0.1414	0.5453	0.1467	0.2076

Table 3. Torsional damping with/without SEDC under the evaluation conditions

b. Tripping and reclosing of one Shangdu-Chengde line

This test was also performed with and without SEDC, respectively. At the initial state, both Shangdu-Chengde lines were in service but only one FSCs was switched on (i.e., k1, k3, k4 were closed and k2 was open, see Fig.2). Breaker k3 was first opened to trip one Shangdu-Chengde line and then reclosed after five seconds. This test was meant to check the system response under the 3-machine and one-line condition. Fig.8 illustrates the dynamics of mode 2 during the operation. It can be seen that during the short period of the 3-machine one-line condition, without SEDC, unit 1 and 2 suffered diverging SSR; while for unit 4 the torsional oscillation converges, but with a very weak damping ratio. The reason is that units 1/2 have a higher mode-2 frequency than units 3/4 (see Table 2) and thus are exposed to a greater SSR risk in this operating condition. If SEDCs were applied, however, the torsional oscillation can be damped out soon and the SSR risk is avoided effectively for all units online.

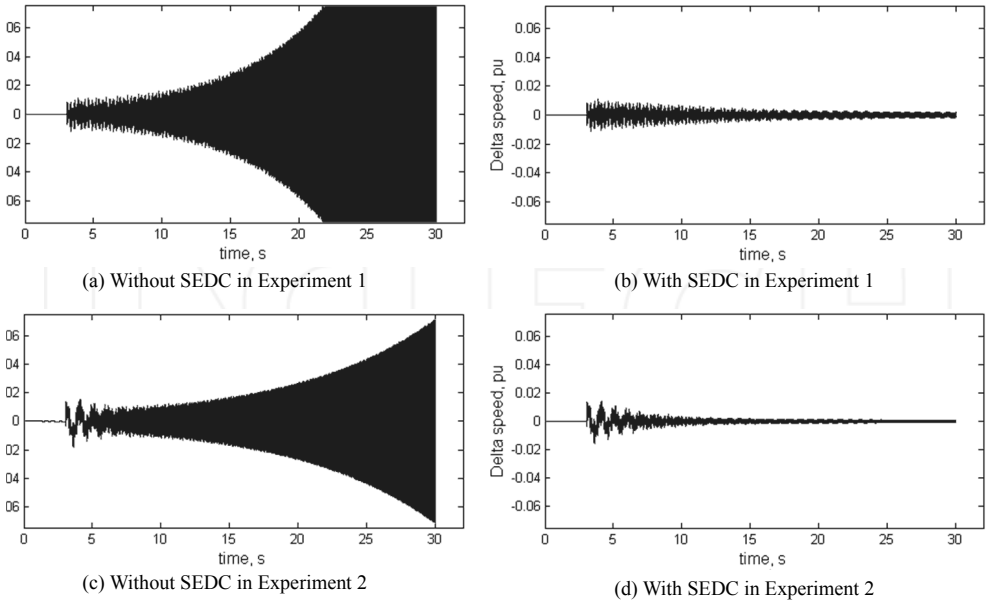

Figure 6. Delta mechanical speed of the high-pressure turbine

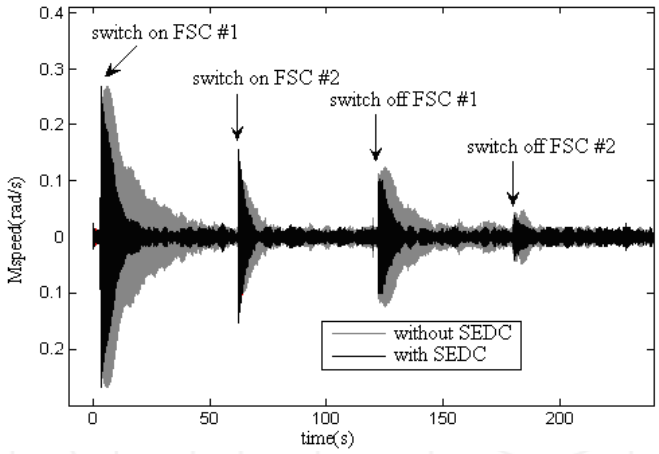

Figure 7. Dynamics of mode 2 during FSCs' switching-on/off operations under the 3-machine condition (unit 4)

From the results of the field tests, it can be concluded that:

i. There is real danger of SSR for the Shangdu series-compensated system, especially for mode 2, which exhibits instability when three or four machines are online while only one Shangdu-Chengde line is in service.

ii. With SEDC applied, the damping of all torsional modes is significantly improved so that the unstable modes become stabilized, which guarantees the safety of the generator shaft and the stability of the system.
iii. The field test includes various operations and covers different working conditions. Especially, the most dangerous conditions previously recognized (i.e., the condition of three/four machine and one Shangdu-Chengdu line) were tested sufficiently. Therefore the effectiveness as well as the robustness of SEDC is very well validated.

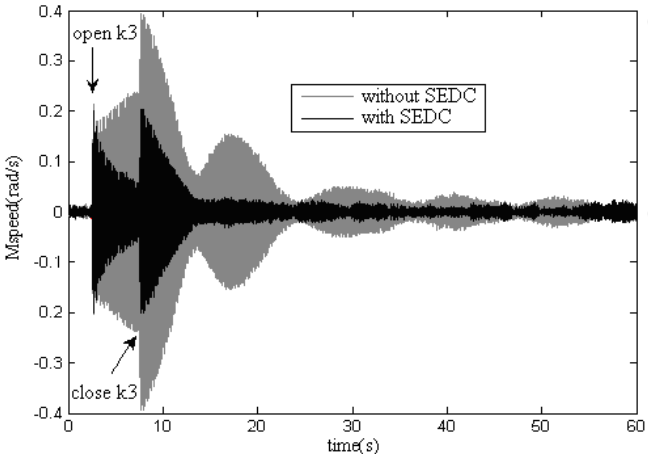

Figure 8. Dynamics of mode 2 during switching operations of Shang-Cheng line #1 under the 3-machine condition (unit 1)

4. Application of GA-SA for SVC-SSDC optimization

4.1. A description of the target system and the multimodal SSR problem

The Jinjie Power Plant is located near Yulin city, Shanxi Province, about 500 kilometers west of Beijing city. As a mine-mouth power plant, it has four 600 MW turbine-generators connected to the North China Power Grid through 500 kV transmissions. Fig. 9 illustrates the one-line diagram of the equivalent system. To improve the transferring capability, 35% SC is applied to the parallel lines between Jinjie Power Plant, Xinzhou substation and Shibei substation. The neighboring Fugu Power Plant, with two 600 MW turbine-generators, is connected to the Xinzhou substation through two uncompensated lines.

Each of Jinjie and Fugu turbine-generators consists of four rotors, i.e., a high-and-intermediate-pressure (HIP) turbine rotor, two low-pressure (LPA/LPB) turbine rotors and the generator rotor, thus resulting in three subsynchronous torsional modes. The modal frequencies were measured via field test and they are about 13.11 Hz (mode 1), 22.77 Hz (mode 2) and 28.22 Hz (mode 3) respectively.

Similarly, a thorough evaluation of the SSR problem was conducted under all possible system conditions for the Jinjie system. As part of the results of eigenvalue analyses, Table 4

gives a list of the real parts, or modal damping, of the three SSR modes under the 4-machine operating conditions (with different load levels and line status, see the "No SVC" column). Thus, the severity of SSR is quantified and the most risky situations are identified.

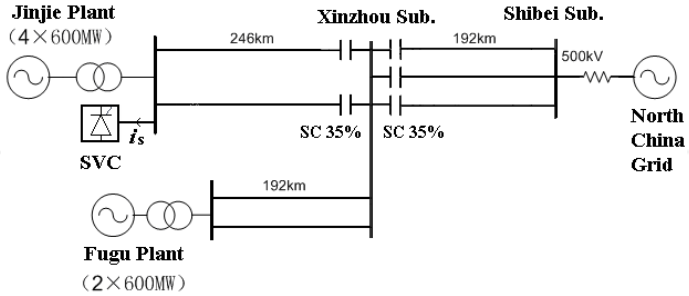

Figure 9. The one-line diagram of the equivalent transmission system

Oper. Con.		Mode 1 (s^{-1})	Mode 2 (s^{-1})	Mode 3 (s^{-1})
Gen. output	lines			
4×0%	2+3	-0.0370	-0.0060	**0.3202**
4×40%	2+3	-0.0378	-0.0262	**0.3099**
4×100%	2+3	-0.0367	-0.0468	**0.3062**
4×0%	2+2	-0.0323	**0.0001**	**0.5708**
4×40%	2+2	-0.0333	-0.0200	**0.5620**
4×100%	2+2	-0.0326	-0.0404	**0.5649**
4×0%	1+3	-0.0156	**0.0223**	**0.3795**
4×40%	1+3	-0.0175	-0.0023	**0.3620**
4×100%	1+3	-0.0182	-0.01760	**0.3480**
4×0%	1+2	-0.0132	**0.0305**	**0.2301**
4×40%	1+2	-0.0152	-0.0105	**0.2108**
4×100%	1+2	-0.0161	-0.0090	**0.1902**

Table 4. Real Parts of SSR modes without and with SVC-SSDC under the 4-machine operating conditions (Note: The "m+n" of the "lines" column means that there are "m" Jinjie-Xinzhou lines and "n" Jinzhou-Shibei lines in service.)

Through the evaluation study, characteristics of the SSR problem are summarized as follows:

i. Mode 1 is well-damped in all operating conditions. Mode 2 is stable in most common operating conditions. However, it becomes weakly-damped or even unstable in some conditions when the generator output is relatively low (corresponding to a lower mechanical damping) or a part of the transmissions are out of service. Mode 3 is the worst damped and tends to be unstable for a number of operating conditions. Thus the SSR problem is a multimodal one.
ii. Modal damping is affected by several factors, including the number of online generators and lines as well as the generators' output. What's more, each torsional

mode has a unique least damped condition, making it a challenge to design a controller adaptable to all operating conditions.

4.2. The SVC-based subsynchronous damping control

Various countermeasures, including the blocking filter, SEDC and SVC were considered to handle the SSR problem of the system. However, SVC was finally chosen as the SSR-depressing device through detailed study and technical versus economic comparison.

4.2.1. The power-electronic circuit and mathematical model of SVC

The adopted six-pulse SVC (see Fig. 10) comprises a thyristor controlled reactor (TCR) and a passive LC filter tuned for the 5th harmonics. It is connected to the high-voltage (500kV) side of the power plant through a step-up transformer.

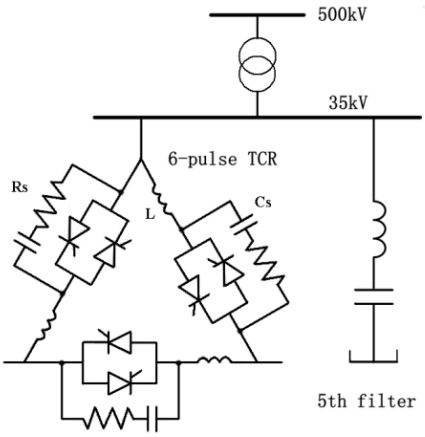

Figure 10. The power-electronic circuit of the six-pulse SVC

Since its MW loss (generally less than 0.6%) is negligible, SVC can be modeled as a controllable inductive admittance [21]. Fig. 11 illustrates the control scheme and mathematical model that describes the dynamics of the fundamental admittance, wherein SVC circuit is represented by combination of a first-order plus dead-time model and a nonlinear function $f(\alpha)$, in series, i.e.

$$f(\alpha) = 1/\left[1/(B_{\mathrm{TCR}} + B_{\mathrm{FLT}}) - X_{\mathrm{T}}\right],\ B_{\mathrm{TCR}} = \left[2\alpha + \sin(2\alpha) - \pi\right]/(\pi X_{\mathrm{L}}),\ 0 \le \alpha \le 0.5\pi \tag{7}$$

where α is the firing angle as determined by the reference $B_{1\mathrm{ref}}$ and $f^{-1}(\alpha)$; X_{T} is the transformer reactance, B_{TCR}, B_{FLT} are admittances of the TCR and the filter; X_{L} is the full reactance of the TCR.

With some simplification, the dynamics of fundamental admittance can be expressed concisely by:

$$B_1 = \frac{e^{-sT_d}}{1+sT_s} B_{1ref}, \quad B_1 \in [\frac{-(1-B_{FLT}X_L)}{X_T(1-B_{FLT}X_L)+X_L}, 0] \tag{8}$$

where T_d and T_s represent the dead and delay times of the thyristor circuits. For the six-pulse SVC, generally $T_d = T_0 / 24$, $T_s = T_0 / 6$ and T_0=0.02 second.

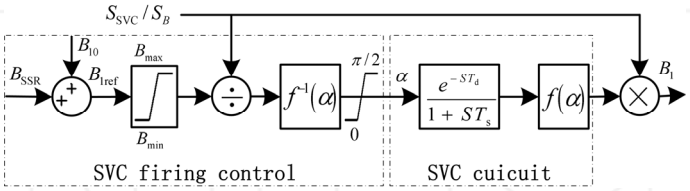

Figure 11. The dynamic model of the SVC

To depress SSR, it is necessary for SVC to generate currents at the complementary subsynchronous frequencies. For this purpose, we propose the idea of modulating the fundamental admittance with subsynchronous frequencies, i.e., to make the reference value of the fundamental admittance (B_{1ref}) vary according to the subsynchronous frequencies, or

$$B_{1ref} = B_{10,ref} + B_{SSR}, \quad B_{SSR} = \sum_{m=1}^{3} B_{1m}(t)\cos(\omega_m t + \varphi_{m,ref}) \tag{9}$$

where $B_{10,ref}$, B_{SSR} denote the DC and subsynchronously modulated components of B_{1ref}; ω_m is the torsional frequency; $\varphi_{m,ref}$ is the initial phase.

Thus, by some derivation, the current of SVC can be derived as

$$i_S = i_1 + \sum_{m=1}^{3} i_{\omega_0-\omega_m} + \sum_{m=1}^{3} i_{\omega_0+\omega_m} + \sum_{k=1}^{\infty}\left(i_{pk\pm1} + i_{(pk\pm1)\omega_0 \mp \omega_m}\right) + i_{else} \tag{10}$$

where $i_1 = U_1 B_{10}\cos(\omega_0 t)$ is the fundamental current; $i_{\omega_0 \mp \omega_m} = 0.5U_1 B_{1m}(t)\cos[(\omega_0 \mp \omega_m)t \mp \varphi_m]$ are the sub- and super- synchronous currents; $i_{pk\pm1}$ denotes the characteristic harmonics; $i_{(pk\pm1)\omega_0 \mp \omega_m}$ are fractional harmonics caused by the subsynchronous modulating control; i_{else} represents the rest of the negligible components; and U_1 is fundamental voltage.

It is observed that by modulating the fundamental admittance with subsynchronous frequencies, SVC produces sub- and super- synchronous currents with controllable amplitude and phase, which subsequently generate subsynchronous damping torque on generator shaft. This is the basic principle of SSR mitigation using SVC. As shown in (10), this method simultaneously causes fractional currents.

4.2.2. Configuration of the proposed SVC-SSDC

The proposed SSDC is a real-time control system that works through the SVC power-electronic circuit to inject sub- and super- synchronous currents into the generator-stators and produces damping torque to ease SSR. Fig. 12 shows the block diagram of the 3-path SVC-SSDC designed for the Jinjie system. The average mechanical speed of HIP turbines of the online machines provides the input, which becomes the standard signal $\Delta\omega_{\mathrm{HIP}}$ after proper conditioning. It is then passed to the low- & high-pass filter. Speed signal filtered next proceeds to three separate control paths. Each, tuned to a specific mode, comprises a modal filter, an amplifier k_i and a unity-gain phase-shifter $(1-sT_k)^2/(1+sT_k)^2$ to generate the control signal for the corresponding mode. The control signals of all torsional modes are summarized, clipped and finally added to form the control signal, or B_{SSR}, which drive the SVC circuit as shown in Fig. 12.

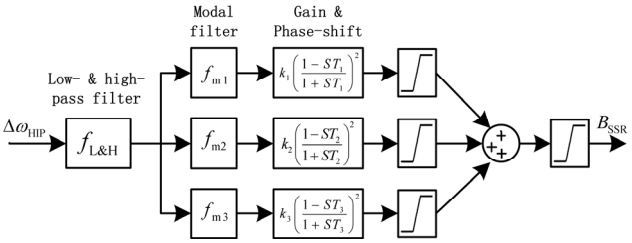

Figure 12. Configuration of SVC-SSDC

The purpose of the low- & high-pass filter, with the transfer functions shown in (11), is to depress the unrelated signals, including the DC, low-frequency (<10Hz) and high-frequency (>40Hz) components, to enable only related subsynchronous signals to pass through.

$$f_{\mathrm{L\&H}}(s)=\frac{1}{1+s/\omega_{\mathrm{L}}+(s/\omega_{\mathrm{L}})^2}\frac{(s/\omega_{\mathrm{H}})^2}{1+s/\omega_{\mathrm{H}}+(s/\omega_{\mathrm{H}})^2},\ \omega_{\mathrm{L}}=2\pi\cdot 40,\quad \omega_{\mathrm{H}}=2\pi\cdot 10 \tag{11}$$

The modal filter is a series combination of a second-order band-pass filter and two second-order band-stop filters, as described in (12):

$$f_{\mathrm{m}\,i}(s)=\frac{s/\omega_{\mathrm{P}i}}{1+8\pi s/\omega_{\mathrm{P}i}^2+(s/\omega_{\mathrm{P}i})^2}\frac{1+(s/\omega_{\mathrm{Bi}1})^2}{1+6\pi s/\omega_{\mathrm{Bi}1}^2+(s/\omega_{\mathrm{Bi}1})^2}\frac{1+(s/\omega_{\mathrm{Bi}2})^2}{1+6\pi s/\omega_{\mathrm{Bi}2}^2+(s/\omega_{\mathrm{Bi}2})^2} \tag{12}$$

where $\omega_{\mathrm{P1}}=\omega_{\mathrm{B21}}=\omega_{\mathrm{B31}}=\omega_1$ =82.38 rad/s, $\omega_{\mathrm{P2}}=\omega_{\mathrm{B11}}=\omega_{\mathrm{B32}}=\omega_2$ =143.07 rad/s, $\omega_{\mathrm{P3}}=\omega_{\mathrm{B12}}=\omega_{\mathrm{B22}}=\omega_3$ =177.33 rad/s.

Then the SVC-SSDC can be reformulated into (13)

$$\Delta B_{\mathrm{SSR}}=H(s)\Delta\omega_{\mathrm{HIP}} \tag{13}$$

where $H(s)$ is the integrated transfer function of SVC-SSDC.

4.2.3. Linearized model of the controlled system

To formulate the control-design problem, the whole system is linearized around a certain operating point to obtain an open-loop linear model [22-24], as described in (14).

$$\Delta\omega_{\mathrm{HIP}} = G(s)\Delta B_{\mathrm{SSR}} \tag{14}$$

where $G(s)$ represents the open-loop transfer function from ΔB_{SSR} to $\Delta\omega_{\mathrm{HIP}}$.

The closed-loop system model is obtained by combining (13) with (14), as shown in Fig.13, where the control reference r is set to 0; d denotes noise and/or model uncertainties. With some manipulation, the transfer functions between the input d and the outputs y, ΔB_{SSR} can be derived as:

$$y(s) = S(s)d(s) \tag{15}$$

$$\Delta B_{\mathrm{SSR}}(s) = R(s)d(s) \tag{16}$$

where $S(s) = \left[1 + G(s)H(s)\right]^{-1}$ is the sensitivity function, and $R(s) = H(s)S(s)$.

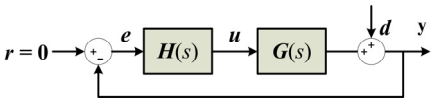

Figure 13. The close-loop system

For the target system, the open-loop and the closed-loop system function, i.e., $G(s), S(s)$ have a maximum order of 93 and 258. Obviously, their poles that correspond to torsional modes represent the stability or damping of these modes for the open-loop and the closed-loop systems, respectively. Hence, by eigen-analysis, the relationship between torsional damping with system variables and SVC-SSDC parameters can be traced out. With pre-determined filtering functions of SVC-SSDC, the selection of gains and phase-shifts or $k_i, T_i (i = 1,2,3)$ in Fig.12 is the key to solve the multimodal SSR problem.

4.3. Optimal design of the SVC-SSDC based on GA-SA

For the target system, sixty representative conditions are selected as the "evaluation conditions" (partly listed in Table 4), which cover the full range of generator output levels as well as the status of transmission lines. While these evaluation conditions by no means limit the situations under which the power system operates, together they form the edge of practical operating conditions and the most unfavorable situations relevant to SVC-SSDC. Therefore, the derived SVC-SSDC is robust enough to stabilize the system under all possible conditions.

The control-design task of SVC-SSDC can also be formulated into a nonlinear constrained optimization problem similar to that of (4)-(5). Specifically, it is expressed by (17)-(18).

$$\begin{aligned} &\max f \\ &\text{subject to: } \left|R(j\omega)\right|_\infty \le R_{\mathrm{m}}, \left|k_i\right| \le k_{\mathrm{ub},i},\ 0 \le T_i \le T_{\mathrm{ub},i} \end{aligned} \tag{17}$$

$$\begin{aligned} &f = \sum_{i=1}^{3} w_i \eta_i + w_4 \min\{\eta_1, \eta_2, \eta_3\}, \sum_{i=1}^{4} w_i = 1, w_i > 0 \\ &\eta_i = \min_{j=1}^{j=60} \left\{\sigma_{ij}\right\},\ \sigma_{ij} = -\mathrm{Re}(\lambda_{ij}) / \left|\mathrm{Im}(\lambda_{ij})\right|, \\ &\lambda_{ij} = \lambda_i \left\{S_j(k_1 \sim k_3, T_1 \sim T_3)\right\}; i = 1,2,3; j = 1,\ldots,60 \end{aligned} \tag{18}$$

where k_i, T_i are control parameters; S_j is the sensitivity function; $\lambda_i\{\cdot\}$ means the calculation of the SSR mode of the included transfer function; the positive weight coefficients $w_1 = w_2 = w_3 = 0.2, w_4 = 0.4$; the subscripts *i*, *j* denote the number of SSR mode and the operating condition respectively.

In (17), $\left|R\right|_\infty$ is the H∞-norm of R, which represents the peak gain of R across all frequencies and can be calculated with the formula (19); R_{m} is the desired maximum value of $\left|R\right|_\infty$; and $k_{\mathrm{ub},i}$, $T_{\mathrm{ub},i}$ are the upper bounds of the gains and time constants.

$$\left|R\right|_\infty = \max_{\omega} \left|R(j\omega)\right| \tag{19}$$

Practically, the output of SSDC is restricted by the SVC capacity. Therefore, to limit the control output and to improve robustness to additive model uncertainty, the transfer function from disturbance to control output, i.e. $R(s)$ in (13), should not be too large. In the other side, SVC rating has great effect on the tuning of control gains and the effectiveness of the closed-loop system. Generally, larger size of SVC leads to higher gains and better torsional damping. However, equipment cost and operation loss increase accordingly. Thus, SVC size was determined for achieved the balance between cost and performance, 240MVA, about 10% of the rated power of all Jinjie machines.

The control-design problem (17)-(18) can be solved again by the proposed GA-SA method. In this case, GA-SA converges to satisfactory results after 40 - 60 iterations, consuming about 10-15 minutes on a modern computer. The optimized SVC-SSDC parameters are listed as follows: $k_1 = 25.46$, $k_2 = -26.03$, $k_3 = 25.02$, $T_1 = 0.0070\mathrm{s}$, $T_2 = 0.0053\mathrm{s}$, $T_3 = 0.0025\mathrm{s}$. The maximum fitness value generated is 0.00185.

4.4. Verification of the optimized SVC-SSDC

4.4.1. Small-signal eigen-analysis

A thorough eigenvalue analysis has been conducted, first in the absence and then in the presence of SVC-SSDC, to check the damping performance of the closed-loop system. Results of the specific operating conditions are presented in Table 5. Comparisons between damping values with and without SVC-SSDC suggest that all torsional modes see

considerable improvement in modal damping by using the optimized SSDC and all unstable modes are well stabilized.

Oper. Con.		Mode 1 (s^{-1})		Mode 2 (s^{-1})		Mode 3 (s^{-1})	
Gen. output	lines	No SVC	With SVC	No SVC	With SVC	No SVC	With SVC
4×0%	2+3	-0.0370	-0.1524	-0.0060	-0.3903	**0.3202**	-0.7235
4×40%	2+3	-0.0378	-0.2174	-0.0262	-0.4796	**0.3099**	-0.6081
4×100%	2+3	-0.0367	-0.3256	-0.0468	-0.5863	**0.3062**	-0.4118
4×0%	2+2	-0.0323	-0.1566	**0.0001**	-0.4559	**0.5708**	-2.0244
4×40%	2+2	-0.0333	-0.2249	-0.0200	-0.5479	**0.5620**	-1.6510
4×100%	2+2	-0.0326	-0.3376	-0.0404	-0.6581	**0.5649**	-1.1766
4×0%	1+3	-0.0156	-0.1596	**0.0223**	-0.6877	**0.3795**	-0.5840
4×40%	1+3	-0.0175	-0.2437	-0.0023	-0.7942	**0.3620**	-0.8436
4×100%	1+3	-0.0182	-0.3792	-0.01760	-0.9205	**0.3480**	-1.2701
4×0%	1+2	-0.0132	-0.1645	**0.0305**	-0.7615	**0.2301**	-0.4166
4×40%	1+2	-0.0152	-0.2495	-0.0105	-0.8712	**0.2108**	-0.6349
4×100%	1+2	-0.0161	-0.3864	-0.0090	-1.0017	**0.1902**	-0.9860

Table 5. Real Parts of SSR modes without and with SVC-SSDC under the 4-machine operating conditions (Note: The "m+n" of the "lines" column means that there are "m" Jinjie-Xinzhou lines and "n" Jinzhou-Shibei lines in service.)

4.4.2. EMT study with real-time digital simulator

To further investigate the performance of the proposed control scheme, real SSDC controllers were developed using digital signal processors. The controllers were then connected to real-time digital simulator (RTDS), which thoroughly incorporated all system nonlinearities, including the power electronic SVC. Real-time electromagnetic simulations were conducted to check the response of the controlled system in the presence of various disturbances to validate the effectiveness of the developed controllers. Some typical results are presented here.

Preliminary study shows that, when only three Xin-Shi SCs are in service, the system is SSR-stable. However, once Jin-Xin SCs are switched on, the system becomes unstable. Fig. 14 depicts the responses of the system during consecutive switch-ons of two Jin-Xin SCs and SVC-SSDC. At the initial stage, Xin-Shi SCs are in service while Jin-Xin SCs and SVC-SSDC are out of service. When #1 Jin-Xin SC is switched on, the system is still stable, as indicated by the converging speed deviation in Fig.14(a). However, once #2 Jin-Xin SC is added in, SSR diverges rapidly and the generators experience violent torsional vibration, as indicated by the exponentially growing delta mechanical speed. This would probably lead to great damage to generator shafts. When SVC-SSDC is applied, SSR attenuates immediately. Fig.14(b) shows the current component of TCR corresponding to torsional mode 3, which is the most intractable among the three SSR modes.

To test the SVC-SSDC in the presence of large disturbances, a three-phase short-circuit is triggered first on the SSDC-free and then, on the SSDC-controlled system. The results are illustrated in Fig. 15.

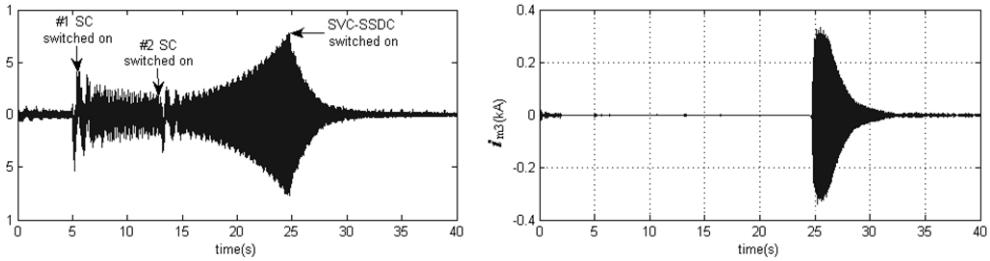

(a) Delta mechanical speed of the HIP turbine (b) The mode- 3component of TCR current

Figure 14. System response during the switching of the Jin-Xin SCs and SVC-SSDC

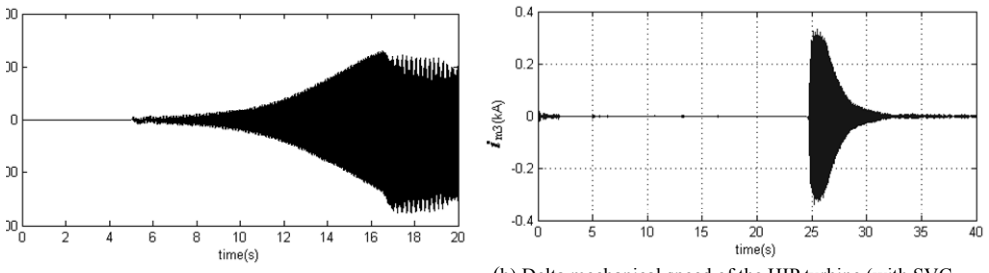

(a) Delta mechanical speed of the HIP turbine (without SVC-SSDC)

(b) Delta mechanical speed of the HIP turbine (with SVC-SSDC)

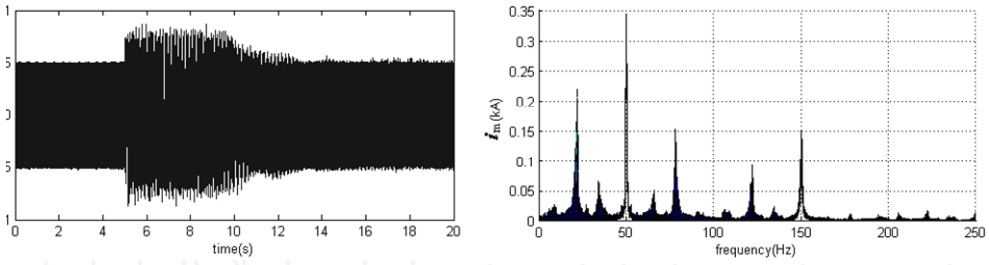

(c) TCR current (with SVC-SSDC)

(d) Spectrum of TCR current (with SVC-SSDC)

Figure 15. System response following a three-phase fault

As shown in Fig.15 (a), in the absence of SSDC, the faulted system is unstable and soon collapses. However, when SVC-SSDC is put into service, the subsynchronous oscillation is successfully damped out (see Fig.15(b)). Fig.15(c) displays SVC's current output during the experiment. For a short period of time after the fault (about 5 seconds), the magnitude of the feedback is so large that the SSDC works nearly in a "bang-bang" mode due to the intense impact of the fault. As the vibration is weakened, the SSDC output becomes attenuated accordingly. From the spectrum of the TCR current shown in Fig.15(d), it can be seen that

during the controlling process, the TCR current contains harmonics at the frequencies of $(2n \pm 1)\omega_0 \pm \omega_m$. This is in line with the previous theoretic analysis.

Besides the exemplary experiment, simulations under other operating conditions have been conducted in the presence of different large disturbances. From Figs.14-15 and other results not presented here, it is concluded that SVC-SSDC is effective in improving torsional damping and can satisfactorily mitigate subsynchronous vibrations caused by any type of disturbance.

5. Conclusions

In this chapter, a novel intelligent tuning technique based on the combined genetic algorithm and simulated annealing, or GA-SA, was proposed and explicated for the design of optimized controllers to depress SSR in practical multi-machine transmission systems compensated with fixed series capacitors. The advantage of the proposed method lies in that: by solving the constrained optimization problem, the multiple control parameters are simultaneously optimized and the obtained controller is robustified to damp multimodal SSR under a wide range of operating conditions. The proposed method is applied to the control-design problems of two practical power systems, i.e., SEDC of the Shangdu system and SVC-SSDC of the Jinjie system. The dynamics of the controlled system are investigated via eigenvalue analyses, electromagnetic simulation and/or field tests, the results of which fully demonstrate the effectiveness of the GA-SA tuned controllers.

Author details

Xiaorong Xie
State Key Lab. of Power System, Department of Electrical Engineering, Tsinghua University, Beijing, China

Acknowledgement

This work was supported in part by National Natural Science Foundation of China (Grant No. 51077080 and 51037002) and State Key Lab. of Power System (Grant No.SKLD11M02).

6. References

[1] Subsynchronous Resonance Working Group of the System Dynamic Performance Subcommittee. Reader's guide to subsynchronous resonance Power Systems. *IEEE Trans.Power System*. 1992; 7(1):150-157.

[2] J. W. Balance, S. Goldberg. Subsynchronous resonance in series compensated transmission lines. *IEEE Trans. Power Apparatus and Systems*. 1973, 92(5): 1649-1658.

[3] IEEE Committee Report. A bibliography for study of subsynchronous resonance between rotating machines and power systems. *IEEE Trans. Power Apparatus and Systems*. 1976, 95(1): 216-218.

[4] IEEE Committee Report. First supplement to a bibliography for study of subsynchronous resonance between rotating machines and power systems. *IEEE Trans. Power Apparatus and Systems*. 1979, 98(6): 1872-1875.

[5] IEEE Committee Report. Second supplement to a bibliography for study of subsynchronous resonance between rotating machines and power systems. *IEEE Trans. Power Apparatus and Systems*. 1985, 104(2): 321-327.

[6] IEEE Committee Report. Third supplement to a bibliography for study of subsynchronous resonance between rotating machines and power systems. paper no. 90 SM 328-5-PWRS presented at the PES Summer Meeting, Minneapolis, Minnesota, July 1990.

[7] IEEE Subsynchronous Resonance Working Group of the System Dynamic Performance Subcommittee Power System Engineering Committee. Countermeasures to subsynchronous resonance problems. *IEEE Trans. Power Apparatus and Systems*. 1980; 99(5): 1810-1818.

[8] IEEE Committee Report, Terms, definitions and symbols for subsynchronous oscillations. IEEE Trans. Power Apparatus and Systems. 1985, 104(3): 1326-1334.

[9] V. Pottakulath, E. P. Cheriyan, R. S. Kumar. Synthesis of power system model for SSR analysis. in *Proc. TENCON 2010 IEEE Region 10 Conf.*, 2010, pp. 545–550.

[10] P. M. Anderson, B. L. Agrawal, J. E. Van Ness, *Subsynchronous Resonance in Power Systems*. New York, NY: Wiley-IEEE Press, Feb., 1999.

[11] Liwei Wang, J. Jatskevich, H. W. Dommel, Re-examination of synchronous machine modeling techniques for electromagnetic transient simulations. *IEEE Trans. Power Systems*, 2007, 22(3): 1221–1230.

[12] U. Karaagac, J. Mahseredjian, O. Saad, S. Dennetiere. Synchronous machine modeling precision and efficiency in electromagnetic transients. *IEEE Trans. Power Delivery*, 2011, 26(2): 1072-1082.

[13] Donghui Zhang, Xiaorong Xie, Shiyu Liu, Shuqing Zhang. An intelligently optimized SEDC for multimodal SSR mitigation. *Electric Power Systems Research 2009*, 79(7): 1018-1024.

[14] Kit Po Wong, Yin Wa Wong. Combined genetic algorithm/simulated annealing/fuzzy set approach to short-term generation scheduling with take-or-pay fuel contract. *IEEE Transactions on Power System* 1996; 11(1): 128-136.

[15] Mantawy AH, Abdel-Magid YL, Selim SZ. Integrating genetic algorithms, tabu search, and simulated annealing for the unit commitment problem. *IEEE Transactions on Power Systems* 1999; 14(3): 829-836.

[16] Thompson M, Fidler JK. Application of the genetic algorithm and simulated annealing to LC filter tuning. *IEE Proceedings-Circuits Devices and System* 2001; 148(4): 177-182.

[17] Tang Renyuan, Yang Shiyou, Li Yan; Wen Geng, Mei Tiemin. Combined strategy of improved simulated annealing and genetic algorithm for inverse problem. IEEE Transactions on Magnetics 1996; 32(3): 1326-1329.

[18] Lee YK, Mohamed PS. A real-coded genetic algorithm involving a hybrid crossover method for power plant control system design. in *Proceedings of 2002 Congress on Evolutionary Computation*, pp.1069– 1074, Honolulu, Hawaii 2002.

[19] X. Xie, X. Guo, Y. Han. Mitigation of multimodal SSR using SEDC in the Shangdu series-compensated power system. *IEEE Trans. Power Systems*, 2011, 26(1): 384-391.

[20] Donghui Zhang, Xiaorong Xie, Shiyu Liu, Shuqing Zhang. An Intelligently Optimized SEDC for Multimodal SSR Mitigation. *Electric Power Systems Research*, 2009, vol. 7: 1018-1024.

[21] Hammad AE, El-Sadek M. Application of a thyristor-controlled var compensator for damping subsynchronous oscillations in power systems. *IEEE Trans. Power Apparatus and Systems*. 1984; 103(1): 198-206.

[22] Putman TH, Ramey DG. Theory of the modulated reactance solution for subsynchronous resonance. *IEEE Trans. Power Apparatus and Systems*. 1982; 101(6): 1527-1535.

[23] Hammad AE, El-Sadek M. Application of a thyristor-controlled var compensator for damping subsynchronous oscillations in power systems. *IEEE Trans. Power Apparatus and Systems*. 1984; 103(1): 198-206.

[24] Wang L, Hsu YY. Damping of subsynchronous resonance using excitation controllers and static var compensators: a comparative study. *IEEE Trans. Energy Conversion*. 1983; 3(1): 6-13.